

This is a self-archived version of an original article. This version may differ from the original in pagination and typographic details.

Author(s): Pérez de Rada, A.; Cano-Ott, D.; Martínez, T.; Alcayne, V.; Mendoza, E.; Plaza, J.; Sanchez-Caballero, A.; Villamarín, D.; Äystö, J.; Jokinen, A.; Kankainen, A.; Penttilä, H.; Rinta-Antila, S.; Agramunt, J.; Algora, A.; Domingo-Pardo, C.; Lerendegui-Marco, J.; Taín, J.L.; Banerjee, K.; Bhattacharya, C.; Roy, P.; Calviño, F.; Cortés, G.; Delafosse, C.; Matea, I.; Benito, J.; Alhomaidhi, S.; Mistry, A. K.

Title: β -delayed neutron spectroscopy of 85As with MONSTER

Year: 2023

Version: Published version

Copyright: © The Authors, published by EDP Sciences.

Rights: CC BY 4.0

Rights url: <https://creativecommons.org/licenses/by/4.0/>

Please cite the original version:

Pérez de Rada, A., Cano-Ott, D., Martínez, T., Alcayne, V., Mendoza, E., Plaza, J., Sanchez-Caballero, A., Villamarín, D., Äystö, J., Jokinen, A., Kankainen, A., Penttilä, H., Rinta-Antila, S., Agramunt, J., Algora, A., Domingo-Pardo, C., Lerendegui-Marco, J., Taín, J.L., Banerjee, K., . . . Mistry, A. K. (2023). β -delayed neutron spectroscopy of 85As with MONSTER. In C. M. Mattoon, R. Vogt, J. Escher, & I. Thompson (Eds.), ND 2022 : 15th International Conference on Nuclear Data for Science and Technology (284, Article 02006). EDP Sciences. EPJ Web of Conferences, 284. <https://doi.org/10.1051/epjconf/202328402006>

β -delayed neutron spectroscopy of ^{85}As with MONSTER

A. Pérez de Rada^{1,*}, D. Cano-Ott¹, T. Martínez¹, V. Alcayne¹, E. Mendoza¹, J. Plaza¹, A. Sanchez-Caballero¹, D. Villamarín¹, J. Äystö², A. Jokinen², A. Kankainen², H. Penttilä², S. Rinta-Antila², J. Agramunt³, A. Algora³, C. Domingo-Pardo³, J. Lerendegui-Marco^{3,8}, J.L. Tañá³, K. Banerjee^{4,5}, C. Bhattacharya^{4,5}, P. Roy^{4,5}, F. Calviño⁶, G. Cortés⁶, C. Delafosse^{2,7}, I. Matea⁷, J. Benito⁹, S. Alhomaidhi^{10,11}, and A.K. Mistry^{10,11}

¹Centro de Investigaciones Energéticas, Medioambientales y Tecnológicas (CIEMAT), E-28040 Madrid, Spain

²JYFL, The Accelerator Laboratory of the Department of Physics, University of Jyväskylä, FI-40014 Jyväskylä, Finland

³Instituto de Física Corpuscular (IFIC), CSIC-Universidad de Valencia, E-46071 Valencia, Spain

⁴Variable Energy Cyclotron Centre (VECC), IN-700064 Kolkata, India

⁵Homi Bhabha National Institute (HBNI), Anushakti Nagar, Mumbai IN-400094, India

⁶Universitat Politècnica de Catalunya (UPC), Departamento de Física, E-08034 Barcelona, Spain

⁷IJCLab, Université Paris-Saclay, CNRS/IN2P3, FR-91405 Orsay Cedex, France

⁸Universidad de Sevilla (US), Facultad de Física, E-41012 Sevilla, Spain

⁹Universidad Complutense de Madrid (UCM), Grupo de Física Nuclear, E-28040 Madrid, Spain

¹⁰Institut für Kernphysik, Technische Universität Darmstadt, D-64289 Darmstadt, Germany

¹¹GSI Helmholtzzentrum für Schwerionenforschung, D-64291 Darmstadt, Germany

Abstract. The β -delayed neutron emission in the ^{85}As β -decay has been measured at the IGISOL facility of the Accelerator Laboratory of the University of Jyväskylä (JYFL). The complete β -decay has been studied with a setup which consists of a plastic scintillator, the **MOD**ular Neutron time-of-flight **SpectrometeR** (MONSTER), and two types of γ -rays detectors (HPGe and LaBr₃). The β -delayed neutron energy distribution has been determined by unfolding the TOF spectrum with the iterative Bayesian unfolding method.

1 Introduction

An accurate quantitative understanding of β -delayed neutron emission rates and spectra is necessary for nuclear structure, astrophysics, and reactor applications: β -delayed neutrons provide valuable information on the β -decay process, are needed in network calculations for understanding the stellar nucleosynthesis process, and can improve the understanding of the kinematics and safety of new reactor concepts loaded with new types of fuels.

The field has experienced an increased activity during the last decades [1] thanks to the advances in nuclear experimental techniques and radioactive ion beam facilities producing increased yields of neutron rich isotopes. Accurate measurements of β -delayed neutron emission properties like the emission probability, β -feeding, and energy spectrum from individual precursors are being carried out with advanced neutron detectors [2–4], digital data acquisition systems [5], and high intensity ion beams [6–9].

In this paper, the results obtained in the measurement at the IGISOL facility of the Accelerator Laboratory of the University of Jyväskylä on the β -delayed neutron energy distribution of the ^{85}As β -decay are reported.

The β -decay chain beginning with ^{85}As proceeds along two branches, β and βn , until the stable ^{85}Rb and ^{84}Kr isotopes are reached. The half-life of the ^{85}As β -decay is

2.021 ± 0.010 s. The decay presents a large Q_β window of 9224.5 ± 4.0 keV. The β -delayed neutron emission is possible due to the low neutron separation energy of its daughter nuclei, ^{85}Se , which results in a $Q_{\beta n}$ window of 4687.2 ± 3.6 keV. The P_n value is of 59.4 ± 2.4 % [10].

2 Experimental setup

The complete decay has been studied with the help of a complex setup consisting of a plastic scintillator detector for the emitted β -particles, the **MOD**ular Neutron time-of-flight **SpectrometeR** (MONSTER) [4, 11] for the detection of the β -delayed neutrons, and one EXOGAM HPGe clover and an array of four LaBr₃ crystals for the detection of γ -rays. Figure 1 shows a photo of the whole ensemble. The ^{85}As isotopes were produced by proton-induced fission reactions in a ^{235}U target. The $A = 85$ isobars were separated from the bulk of fission products by the IGISOL dipole magnet with resolution $M/\Delta M = 500$ [9] and implanted on a movable tape inside of the β -detector.

The β -detector consisted of an BC408 cup-like shaped plastic detector wrapped with reflector foil and coupled to an R5924-70 PMT model. It was located on top of the tape system, inside the vacuum pipe, in such a way that the implantation in the tape could take place through a 10 mm aperture on the side of the detector cup.

The MONSTER array used 48 cylindrical cells of 200 mm diameter and 50 mm height, filled with either

*e-mail: alberto.rada@ciemat.es

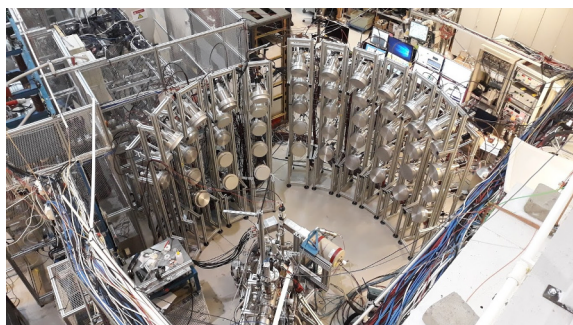


Figure 1. Experimental setup used at the JYFL facility.

BC501A or EJ301 scintillating liquid. Each cell is coupled through a light guide of 31 mm thickness to either a R4144 or R11833 PMT. In this experiment the cells were arranged in two different setups with 30 and 18 cells at 2 and 1.5 m flight paths, respectively.

The signals from the plastic detector and MONSTER are used as the start and stop signals, respectively, to measure the neutrons' time-of-flight (TOF).

All the detector signals were registered with a custom digital data acquisition (DAQ) system developed at CIEMAT based on ADQ14 digitizers from Teledyne SP Devices with 14 bit resolution and 1 GSample/s sampling rate. The complete detector setup required 60 channels.

Custom pulse shape analysis software was developed at CIEMAT to analyze the registered signals online. The β -detector signals were fitted to the average signal in order to resolve pileups. MONSTER signals were analyzed using the digital integration method in different regions. The pulse shape analysis routine does not add any dead time.

The data was collected in cycles of implantation and decay adapted to the half-lives of the isotopes involved for maximizing the activity of the neutron emitter with respect to the other isobars consisting 95 % of the mass separated beam, see Section 4.1. During the cycle, the ion beam was switched on and off by electrostatic deflection at the switchyard of the IGISOL beam line. The cycle also included an initial time interval for background measurement and a final time interval for removal of the long-lived activity of the decay products.

3 Efficiency characterization

The detection efficiency of the different detection systems has been determined by Monte Carlo simulations in combination with experimental measurements that served as validation of the simulations.

In the case of the β -detector, the efficiency has been determined experimentally at two different endpoint energy values from the ^{92}Sr β -decay through the coincidence technique with characteristic γ -rays in the HPGe and LaBr₃ detectors. The Monte Carlo simulations were used for extending the detector efficiency as a function of the endpoint energy and for estimating the detection threshold of 260 keV. The result of the efficiency calculation and the

comparison with the experimental data are shown in Figure 2.

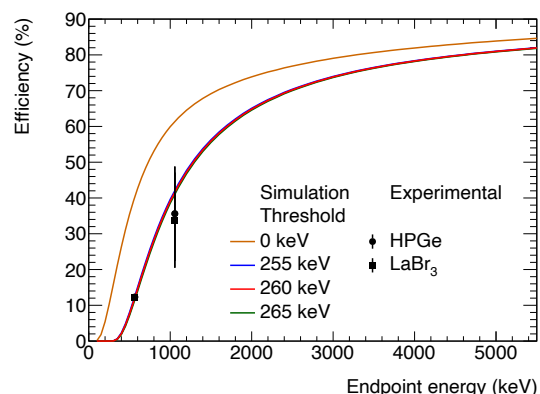


Figure 2. β -efficiency determined from ^{92}Sr β -decay and Monte Carlo simulations. The two values of the first experimental endpoint energy are exactly the same.

The MONSTER neutron detection efficiency has been determined through Monte Carlo simulations and validated with the data from a measurement with a 1.00 ± 0.15 GBq ^{252}Cf source. The γ -rays from the spontaneous fission of ^{252}Cf detected in the LaBr₃ detectors served for establishing a TOF between the emission and the detection of the spontaneous fission neutrons. Neutron signals in MONSTER were selected by performing pulse shape discrimination, which allowed for a background reduction due to γ -rays of one order of magnitude. The response of MONSTER to different neutron energies was obtained by setting different cuts in the γ -neutron TOF spectrum. The Monte Carlo simulations were performed with the light output response obtained from previous calibrations with monochromatic energy neutron beams [11]. As it is shown in Figure 3, there is an excellent agreement between the experimental values and the Monte Carlo simulations of the MONSTER arrays for the two different flight paths.

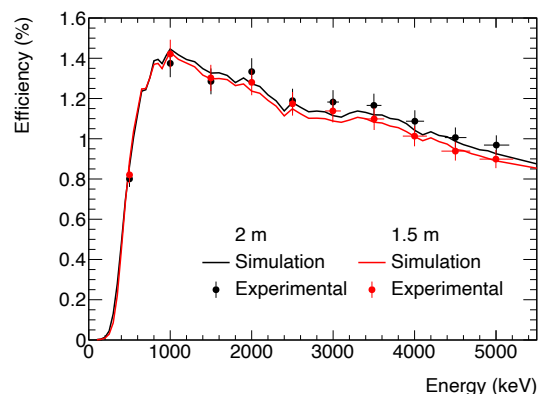


Figure 3. Total neutron detection efficiency for both setups of MONSTER determined from ^{252}Cf and comparison with Monte Carlo simulations.

4 Data analysis and results

The analysis techniques developed and applied for obtaining the results of the measurement [12], as well as the results themselves, are presented in this section.

4.1 Growth and decay curve method

The growth and decay curve method has been applied to determine the implantation rates of the different isotopes being implanted onto the tape and the contributions of their daughters. The time evolution of the β -activity during each cycle due to all isotopes in the decay chain is governed by the Bateman equations. The experimental β -activity distribution is fitted with a function based on the generic solution given in [13] that describes the contribution of each of the isotopes involved in the decay chain:

$$A(t) = \sum_{i=1}^n \bar{\epsilon}_i \lambda_i N_i(t),$$

where $\bar{\epsilon}_i$ is the average efficiency to detect a β -particle coming from the β -decay of the i -th member of the chain, λ_i is the decay constant of the i -th member of the chain, and $N_i(t)$ is the number of nuclei of the i -th member of the chain given by the solution of the Bateman equations, which depends on the respective implantation rate R_i .

The measurement cycle consisted of 3 s of background, 15 s of implantation, and 14 s of decay. Thus, the β -activity curve was fitted taking into account only the contributions of ^{85}As , $^{85,84}\text{Se}$, and ^{85}Br due to the longer half-lives of ^{85}Kr and ^{84}Br . In addition, a constant background contribution was included in the fit. The experimental curve together with the total fit and the individual contributions can be seen in Figure 4.

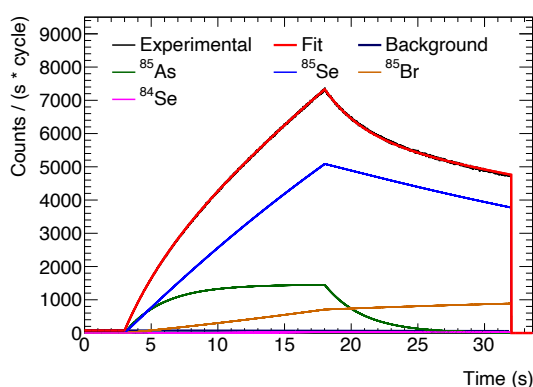


Figure 4. Time evolution of the β -activity and the corresponding fit, including individual isotopes' contributions and a background component.

The results of the fit are presented in Table 1. The other values that are in the table are the calculated average detection efficiencies as well as the total number of decays of each of the isotopes. The average detection efficiencies for each of the β -decays were calculated through Monte Carlo simulations.

Table 1. Results of the fit to the β -activity curve, along with the calculated average efficiencies and the total number of decays.

Isotope	$\bar{\epsilon}$ (%)	R (nuclei/s)	Total decays ($\times 10^6$)
^{85}As	80.8 ± 4.0	1800 ± 100	48 ± 3
^{85}Se	76.0 ± 3.8	23300 ± 900	239 ± 9
^{85}Br	69.7 ± 3.5	13900 ± 2500	42 ± 5
^{84}Se	55.1 ± 2.8	0 ± 0	1.8 ± 0.1

4.2 TOF spectrum unfolding

The neutron energy distribution was determined through the unfolding of the measured neutron TOF spectrum. An innovative analysis procedure based on the iterative Bayesian unfolding method [14] has been developed. According to the iterative Bayesian unfolding method, assuming an initial probability distribution of independent causes (neutron energies) and the probability of each of the causes to produce specific effects (TOF spectrum), the conditional probability of a specific effect (E_j) being due to a certain cause (C_i) is given by:

$$P(C_i|E_j) = \frac{P(E_j|C_i)P_0(C_i)}{\sum_{l=1}^{n_c} P(E_j|C_l)P_0(C_l)}.$$

The conditional probability $P(E_j|C_i)$ is the response matrix of the detection system and can be estimated through Monte Carlo simulations. The construction of the response matrix is crucial to achieve a good result.

The response matrix used to unfold the experimental TOF spectrum obtained with the MONSTER array at 2 m is shown in Figure 5. Each of the causes corresponds to a neutron energy range that has been chosen according to the energy resolution of the system except for the last one, which is a flat background contribution to account for the γ -rays background.

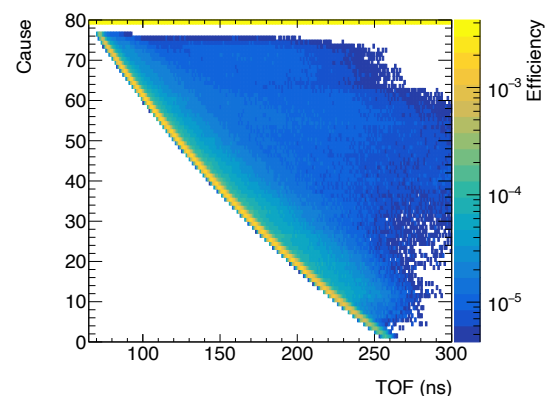


Figure 5. Response matrix for the MONSTER array at 2 m.

Using this response matrix, the experimental TOF spectrum was reconstructed. For the case of the MONSTER array at 2 m, such reconstruction, together with the individual causes, can be seen in Figure 6.

Finally, the neutron energy distributions obtained with both MONSTER arrays are presented in Figure 7. Clearly,

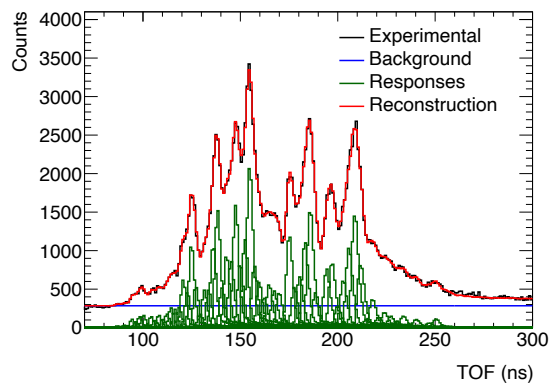


Figure 6. Experimental TOF spectrum together with the reconstruction and the individual causes' contributions.

the agreement of both arrays is excellent within their energy resolution.

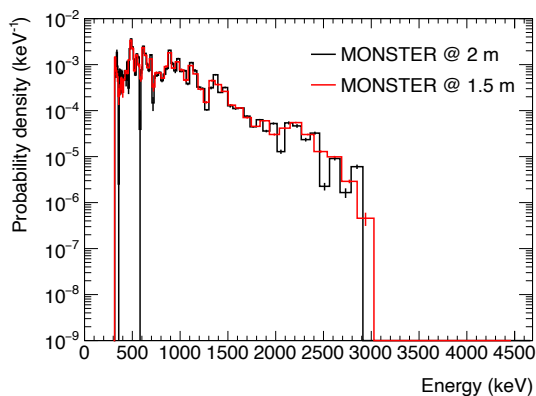


Figure 7. Neutron energy distributions obtained with both MONSTER arrays.

Combining the results obtained from the TOF unfolding and the β -activity fit, P_n values of $40 \pm 4\%$ and $41 \pm 4\%$ are obtained with the MONSTER arrays at 2 and 1.5 m, respectively. These values are lower than the one reported in the bibliography, which is expected due to the neutron energy threshold of around 300 keV of the detection system. However, it can be seen that the results of this work are compatible with existing data [10, 15] in the comparison shown in Figure 8. To make the comparison more straightforward, the existing data has been rebinned to the binning of the results of this work. Also, the obtained energy distribution has been scaled so that the intensities over the experimental threshold are equal. It's worth noting that no neutron intensity over around 3 MeV, which is predicted by calculations, is observed. This could be due to the γ -rays background.

5 Summary

This work entails a successful commissioning and measurement with MONSTER and the custom DAQ and pulse

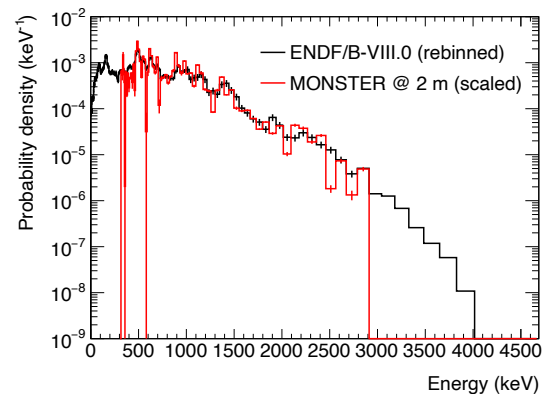


Figure 8. Comparison between the results of this work and existing data.

shape analysis routines. MONSTER is a neutron TOF spectrometer with good neutron/ γ -ray discrimination capabilities and excellent neutron energy resolution.

Accurate Monte Carlo simulations of the complete detection system have been performed and validated by reproducing the efficiency of the different detectors (neutrons and β -particles) with known sources and decays.

An innovative analysis methodology based on the fit of the β -activity curve with the Bateman equations and the unfolding of the neutron TOF spectrum with the iterative Bayesian unfolding method has been developed.

Lastly, the β -delayed neutron energy spectrum of ^{85}As has been procured. This result is in excellent agreement with previous experimental data [15] and evaluations [10].

References

- [1] P. Dimitriou *et al.*, Nucl. Data Sheets, **173**, 144-238 (2021)
- [2] A. Buřa *et al.*, Nucl. Instrum. and Methods A, **455**, 412-423 (2000)
- [3] C. Matei *et al.*, Proc. of the 10th Int. Symp. on Nuclei in the Cosmos, 138, Proceedings of Science, 1-5 (2008)
- [4] A.R. Garcia *et al.*, JINST, **7**, C05012 (2012)
- [5] D. Villamarin *et al.*, In preparation
- [6] W.F. Henning *et al.*, GSI publication (2001)
- [7] H. Okuno, *et al.*, Prog. Theor. Exp. Phys., 03C002 (2012)
- [8] R. Catherall *et al.*, Nucl. Instrum. and Methods B, **317**, 204-207 (2013)
- [9] I.D. Moore *et al.*, Nucl. Instrum. and Methods B, **317**, 208 (2013)
- [10] D.A. Brown *et al.*, Nucl. Data Sheets, **148**, 1-142 (2018)
- [11] T. Martinez *et al.*, Nucl. Data Sheets, **120**, 78 (2014)
- [12] A. Pérez de Rada, PhD Thesis, To be submitted
- [13] K. Skrable *et al.*, Health Physics, **27**, 155-157 (1974)
- [14] G. D'Agostini, Nucl. Instrum. and Methods A, **362**, 487-498 (1995)
- [15] K.-L. Kratz *et al.*, Nucl. Phys. A, **317**, 335 (1979)